Opto-Electronic Engineering

Review

2022 年, 第 49 卷, 第 9 期

DOI: 10.12086/oee.2022.220021

前向受激布里渊散射光纤传感研究进展

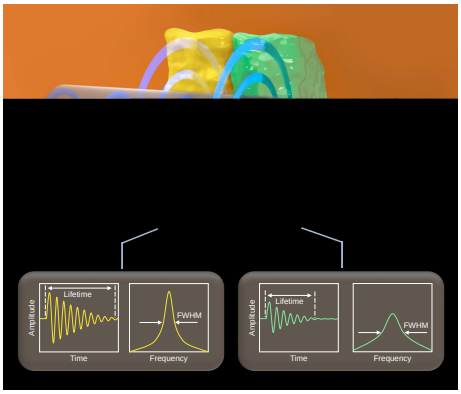

李天夫[1]，巴德欣[1]，周登望[1,2]，任玉丽[1]，
陈　超[1]，张洪英[3]，董永康[1*]

[1] ( )
150001

[2]
150001

[3]
150080

摘要：前向受激布里渊散射 (F-SBS) 是光纤中重要的三阶非线性效应，是进行外界物质识别和分析研究光纤物理特性的有力手段，成为近年研究的热点。本文通过对光纤中前向受激布里渊散射研究进展的调研和分析，整合了 F-SBS 的主要理论和传感原理，回顾了基于相位解调和能量转移探测的 F-SBS 测量手段，并重点介绍了本地光相位追溯技术、光力时域反射技术和光力时域分析技术等分布式传感技术。随着 F-SBS 传感器的逐渐实用化，对于 F-SBS 的高精度、高空间分辨力分布式测量的需求愈发显著，这将是未来光纤中前向受激布里渊散射的主要研究方向。

关键词：前向受激布里渊散射；光纤传感；光力时域分析；非线性光学

中图分类号：TP212；TN253　　**文献标志码：**A

. [J]. 2022 **49**(9): 220021
Li T F, Ba D X, Zhou D W, et al. Recent progress in optical fiber sensing based on forward stimulated Brillouin scattering[J]. *Opto-Electron Eng*, 2022, **49**(9): 220021

Recent progress in optical fiber sensing based on forward stimulated Brillouin scattering

Li Tianfu[1], Ba Dexin[1], Zhou Dengwang[1,2], Ren Yuli[1], Chen Chao[1], Zhang Hongying[3], Dong Yongkang[1*]

[1] National Key Laboratory of Science and Technology on Tunable Laser, Harbin Institute of Technology, Harbin, Heilongjiang 150001, China;

[2] Postdoctoral Research Station for Optical Engineering & Research Center for Space Optical Engineering, Harbin Institute of Technology, Harbin, Heilongjiang 150001, China;

[3] Heilongjiang Provincial Key Laboratory of Quantum Control, School of Measurement and Communication Engineering, Harbin University of Science and Technology, Harbin, Heilongjiang 150080, China

收稿日期：2022−03−19；收到修改稿日期：2022−06−11
基金项目：　(62075051　61975045)　(LH2020F014
*通信作者：　aldendong@163.com

Abstract: Forward stimulated Brillouin scattering (F-SBS), a 3-order nonlinear effect in optical fibers, has become the hotspot in recent years, due to its great potential in substance identification, and fiber diameter measurement, etc. Through research and analysis of the progress of F-SBS, the main principle and key techniques are generalized in this paper. Distributed sensing schemes based on local light phase recovery, opto-mechanical time-domain reflectometry, and opto-mechanical time-domain analysis are emphatically introduced here. With the gradual practical application of F-SBS, the demand for distributed measurement of F-SBS with high precision and high spatial resolution becomes more and more significant, which will be the main research direction of F-SBS in optical fibers in the future.

Keywords: forward stimulated Brillouin scattering; optical fiber sensing; opto-mechanical time-domain analysis; nonlinear optics

1 引 言

[1-6]

[7-9]

(forward stimulated Brillouin scattering, F-SBS)

F-SBS [10]

F-SBS

[11]

F-SBS

[12] F-SBS

[13] [14-15]

F-SBS F-SBS

F-SBS

F-SBS

2 前向受激布里渊散射的基本原理

2.1 F-SBS 的发展概述和基本原理

1922

Brillouin Léon [16]

1930 Gross

[17]

[18]

[19]

(backward stimulated Brillouin scattering, B-SBS)

(Brillouin optical time domain analysis, BOTDA)[20]

(Brillouin optical correlation domain analysis, BOCDA)[21]

[22-25]

ν_B

$$\nu_B = \frac{\Omega_B}{2\pi} = \frac{2nV_A}{\lambda_p}\sin\frac{\theta}{2}, \quad (1)$$

Ω_B n V_A

λ_p θ

$\theta = 180°$

$\theta = 0°$ 0

$(\omega_p, \boldsymbol{k}_p)$ $(\omega_s, \boldsymbol{k}_s)$

$(\Omega_B, \boldsymbol{q})$

1(a)

$$\begin{aligned}\omega_p &= \omega_s + \Omega_B \\ \boldsymbol{k}_p &= \boldsymbol{k}_s + \boldsymbol{q}\end{aligned} \quad . \quad (2)$$

B-SBS

x (

)

F-SBS

1(b)

1985 Shelby

(guided acoustic-wave Brillouin scattering, GAWBS) [10] F-SBS

“not predicted ( )”

F-SBS

B-SBS F-SBS

(transverse acoustic wave, TAW)

[26-27]

n

J_n n

$n = 0$

(radial mode, $R_{0,m}$) $R_{0,m}$ F-SBS

GAWBS

$$\left(1-\alpha^2\right)J_0(y) - \alpha^2 J_2(y) = 0, \quad (3)$$

$$\omega_m = v_L\sqrt{k^2 + \frac{y_m{}^2}{r^2}}. \quad (4)$$

(4) $R_{0,m}$ α

v_T v_L v_T v_L SiO_2 3740

m/s 5996 m/s k r

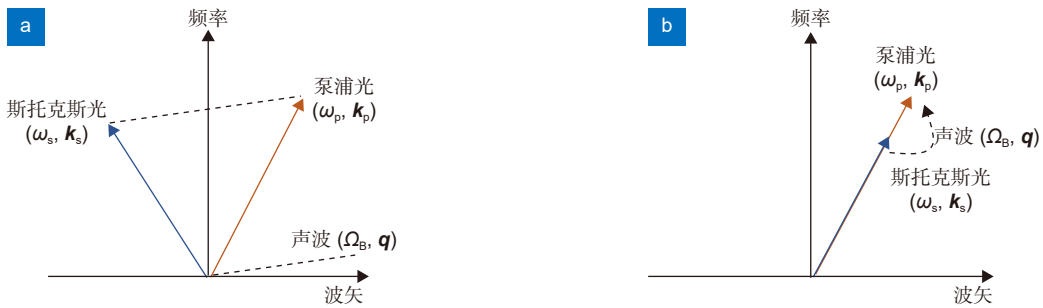

图 1 相位匹配关系。(a) 后向受激布里渊散射; (b) 前向受激布里渊散射

Fig. 1 Phase matching. (a) Backward stimulated Brillouin scattering; (b) Forward stimulated Brillouin scattering

y_m ω_m (3) m $R_{0,m}$ m

0

k 0 $k=0$ (4)

$$\Omega_{0,m}=\frac{v_L y_m^2}{r^2}\,. \tag{5}$$

$\Omega_{0,m}$ $R_{0,m}$ k

0 $\omega_m \approx \Omega_{0,m}$

2 F-SBS

n=2 (4)

(torsional-radial mode, $TR_{2,m}$) [28] $TR_{2,m}$

GAWBS

$$\begin{vmatrix} [(3-y^2/2)J_2(\alpha y)] & [(6-y^2/2)J_2(y)-3yJ_3(y)] \\ [J_2(\alpha y)-\alpha y J_3(\alpha y)] & [(2-y^2/2)J_2(y)+yJ_3(y)] \end{vmatrix}=0\,, \tag{6}$$

$$\Omega_{2,m}=\frac{v_T y_m^2}{r^2}\,. \tag{7}$$

(Standard single-mode fiber, SMF)

$R_{0,m}$ $TR_{2,m}$ 3

- ( ) - ( )

SMF F-SBS m

$R_{0,7}$ 4

$R_{0,m}$ $TR_{2,m}$

$R_{0,m}$

$TR_{2,m}$

$R_{0,m}$ $TR_{2,m}$

3.2

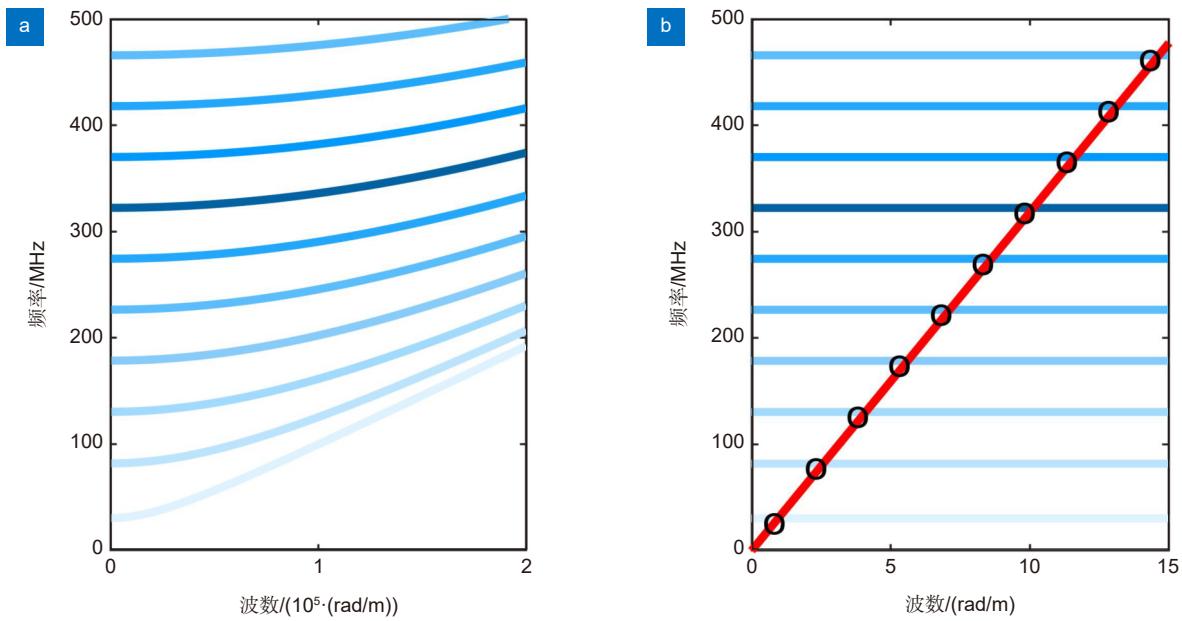

图 2 $R_{0,m}$ 主导的 F-SBS 的色散关系。蓝色曲线为声波的色散曲线，红色曲线为光波的色散曲线，蓝色曲线颜色深浅表示 F-SBS 的作用强度。

Fig. 2 Dispersion relation of $R_{0,m}$-induced F-SBS. The bule solid lines represented the dispersion curve of acoustic waves, and the red one represented which of light wave. The shade of blue lines means the intensity of F-SBS.

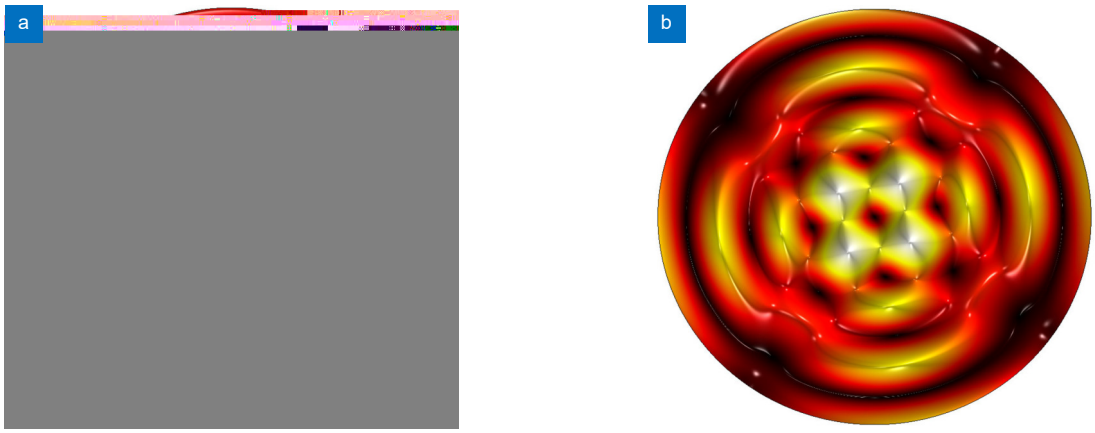

图 3 位移场分布。(a) $R_{0,5}$ 模式; (b) $TR_{2,5}$ 模式

Fig. 3 Transverse displacement profiles. (a) Radial mode $R_{0,5}$; (b) Torsional-radial mode $TR_{2,5}$

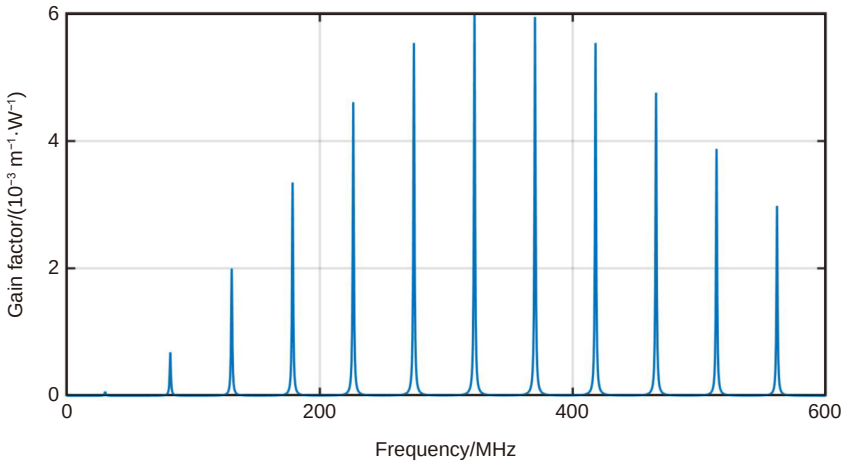

图 4 $R_{0,m}$ 模式驱动的 F-SBS 谱

Fig. 4 Spectrum of $R_{0,m}$ modes induced F-SBS

2.2 前向受激布里渊散射的传感原理

F-SBS

F-SBS B- F-SBS Shelby

SBS B-SBS 1985 [10]

F-

SBS 1998 Tanaka

$TR_{2,5}$ 2011 Wang

[14]

[15]

10 kHz/ 0.194 kHz/με [31] 2016 Antman F-SBS

F-SBS B-SBS (F-SBS

[11]

1.17 MHz/ 0.0478 MHz/με)[29-30] 2.1

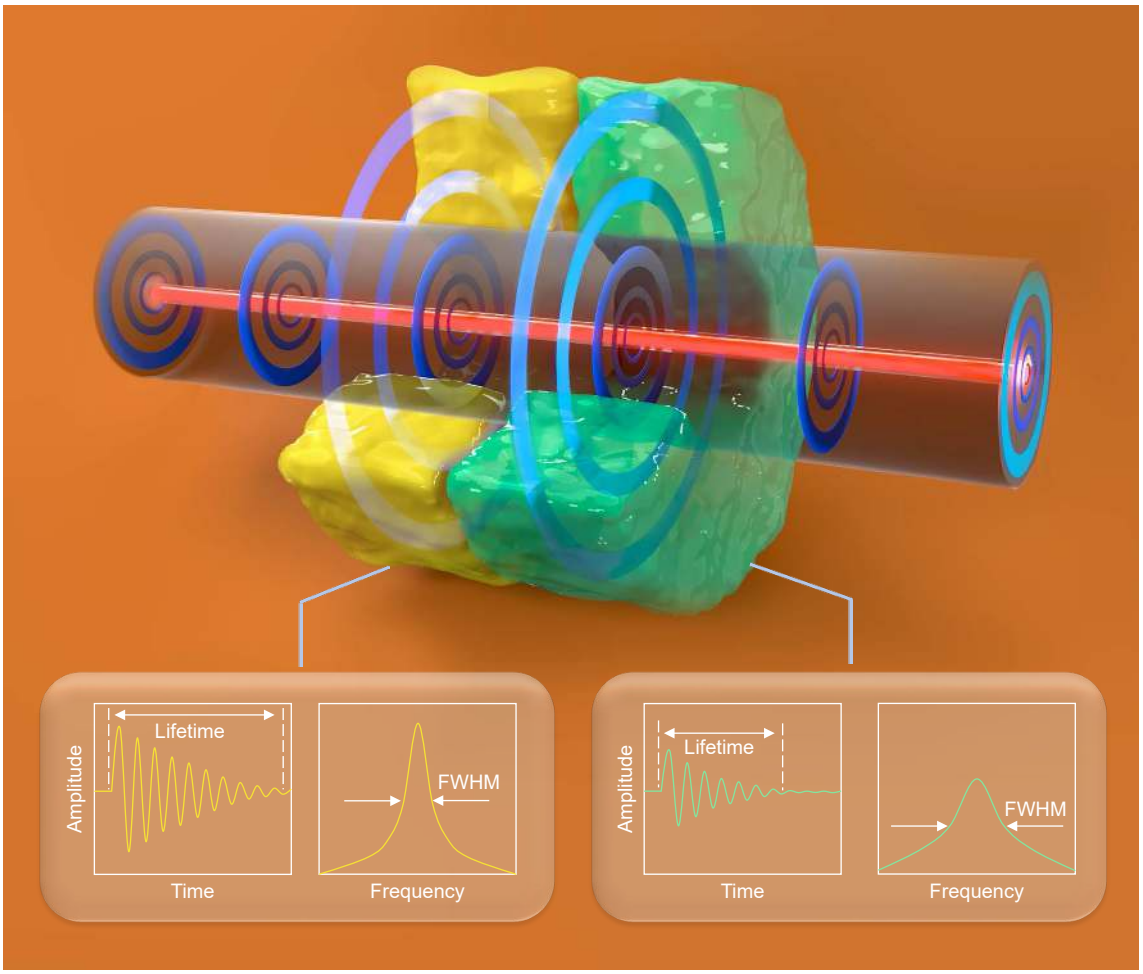

图 5 F-SBS 用于声阻抗传感的原理示意图

Fig. 5 The schematic diagram of acoustic impedance sensing

R

$$R = \frac{\left|Z_{SiO_2} - Z_{outside}\right|}{Z_{SiO_2} + Z_{outside}} , \quad (8)$$

Z_{SiO_2} $Z_{outside}$

τ_{int}

$\Delta\upsilon_s$ (9) (10)

F-SBS 1

- -

(10)

F-SBS $R_{0,m}$ [32-34] (~>50 μm)

τ

$$\frac{1}{\tau} = \frac{1}{\tau_{int}} - \frac{v_L}{2r}\ln(R) , \quad (9)$$

$$\Delta\upsilon = \Delta\upsilon_s - \frac{v_L}{2\pi r}\ln(R) , \quad (10)$$

表 1 常见物质的声阻抗和 SMF 在其中发生 F-SBS 的谱宽

Table 1 Acoustic impedance and F-SBS spectrum width of common substances

	/(kg·m^{-2}·s^{-1})	F-SBS /MHz	
	439.6	0.45	[35]
	0.93×10^6	2.21	[35]
	1.483×10^6	3.57	[36]
NaCl (4%)	1.571×10^6	3.78	[11]
NaCl (8%)	1.664×10^6	4.00	[11]
NaCl (12%)	1.763×10^6	4.24	[11]
( )	3.60×10^6	8.7(2.83)	[32]
( )	3.39×10^6	8.16(~8)	[37]
	13.19×10^6	\	[32]

3 前向受激布里渊散射的探测手段

F-SBS

$R_{0,m}$ F-SBS

$TR_{2,m}$

$R_{0,m}$ [11]

F-SBS

F-SBS

( )

$$Q_{ES} = (a_1 + 4a_2)\cdot\left\langle \nabla_\perp^2 E_0(r)^2 \rho_0(r)\right\rangle , \tag{12}$$

$$Q_{PE} = \left(\frac{a_1}{2} + a_2\right)\cdot\left\langle E_0(r)^2 \rho_0(r)\right\rangle , \tag{13}$$

Q_{ES} $R_{0,m}$

Q_{PE}

$P(\Omega)$ Ω

n $\bar{\rho}$ c

$\Gamma_{0,m}$ $\Omega_{0,m}$ $R_{0,m}$

i $a_1 = -n^4(P_{11} - P_{12})$ $a_2 = -n^4 P_{12}$

P_{11} P_{12} $E_0(r)$ $\rho_0(r)$

$\langle\rangle$

TAW F-SBS

TAW

$$\Delta\varphi(\Omega, L) = k\int_0^L \Delta n(\Omega, z)\,\mathrm{d}z, \tag{14}$$

k L F-SBS

(14)

F-SBS

3.1 基于相位解调的探测方案

$\Delta\varphi$

P

z F-

$$\Delta n(\Omega, z) = \frac{Q_{ES} Q_{PE} P(\Omega)}{4\bar{\rho} n^2 c \Gamma_{0,m} \Omega_{0,m}\left[\mathrm{i} - 2(\Omega - \Omega_{0,m})/\Gamma_{0,m}\right]} , \tag{11}$$

SBS

$g_{0,m}$ F-SBS F-SBS

2009 Kang Sagnac [39]

$$g_{0,m} = \frac{\omega Q_{\mathrm{ES}} Q_{\mathrm{PE}}}{2\bar{\rho} n^2 c^2 \Gamma_{0,m} \Omega_{0,m}} . \qquad (15)$$

7

Shelby - (Mach-Zehnder interferometer, MZI) F-SBS[10]

1.8 μm

10 m

(Sagnac interferometer, SI) F-SBS

SI

F-SBS 6 $(\gamma_{0,1}^{\mathrm{PCF}} = 1.5\ \mathrm{W^{-1}m^{-1}} >> \gamma_{0,6}^{\mathrm{SMF}} = 8\times10^{-3}\ \mathrm{W^{-1}m^{-1}})$

100 ps 6 W

10 GHz

B

$$I = I_{\mathrm{CW}} + I_{\mathrm{CCW}} + 2\sqrt{I_{\mathrm{CW}} \cdot I_{\mathrm{CCW}}} \cos\Delta\varphi , \qquad (16)$$

I_{CW} I_{CCW}

$\Delta\varphi$ F-SBS [42]

2017 Avi Zadok

F-SBS F-SBS

[11,28,33,38-41] [43-44]

F-SBS

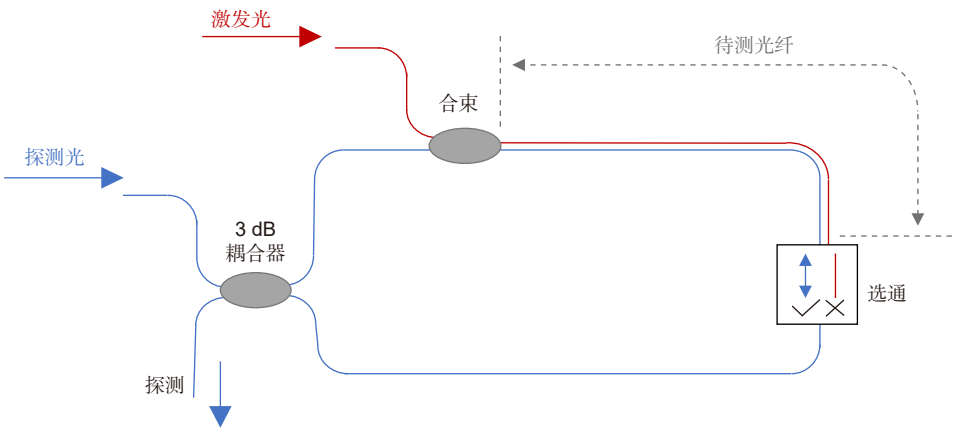

图 6 赛格纳克干涉仪用以测量 F-SBS

Fig. 6 SI used to measure F-SBS

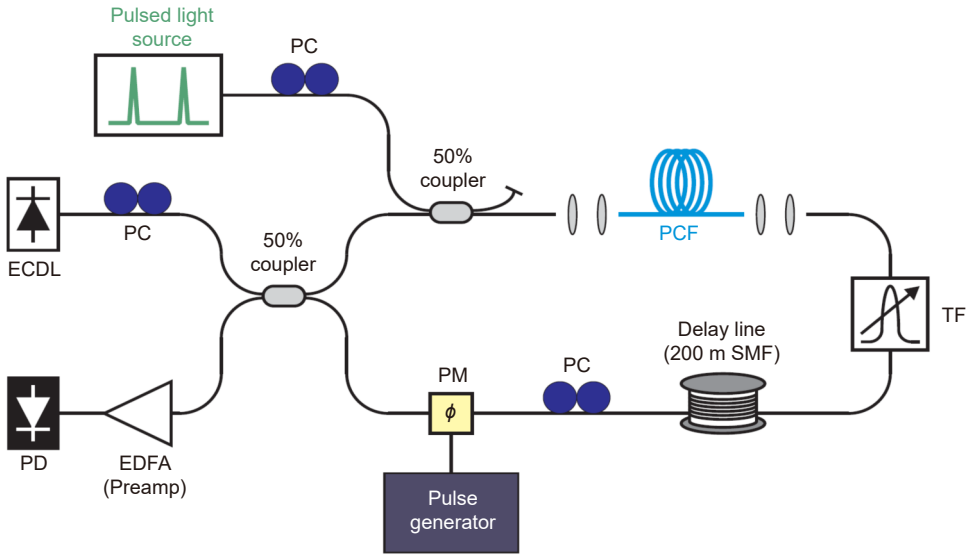

图 7 基于赛格纳克干涉仪的波分泵探 F-SBS 探测方案[39]

Fig. 7 The experimental set-up of F-SBS measurement based on SI. The excitation and probe light are separated by their different wavelengths[39]

$R_{0,m}$ $TR_{2,m}$ F-SBS

F-SBS

F-SBS F-SBS

kW

((W)

8(a) $R_{0,7}$)

(8(b) $R_{0,8}$) 11 cm F-SBS

F-SBS

2021 Zadok

F-SBS [41]

x y

x y

(fiber Bragg grating, FBG) F-SBS

FBG

9

2020 Díez

(long-period grating, LPG) F-

SBS 10 [45] B-

SBS

F-SBS

LPG SMF F-SBS

LPG

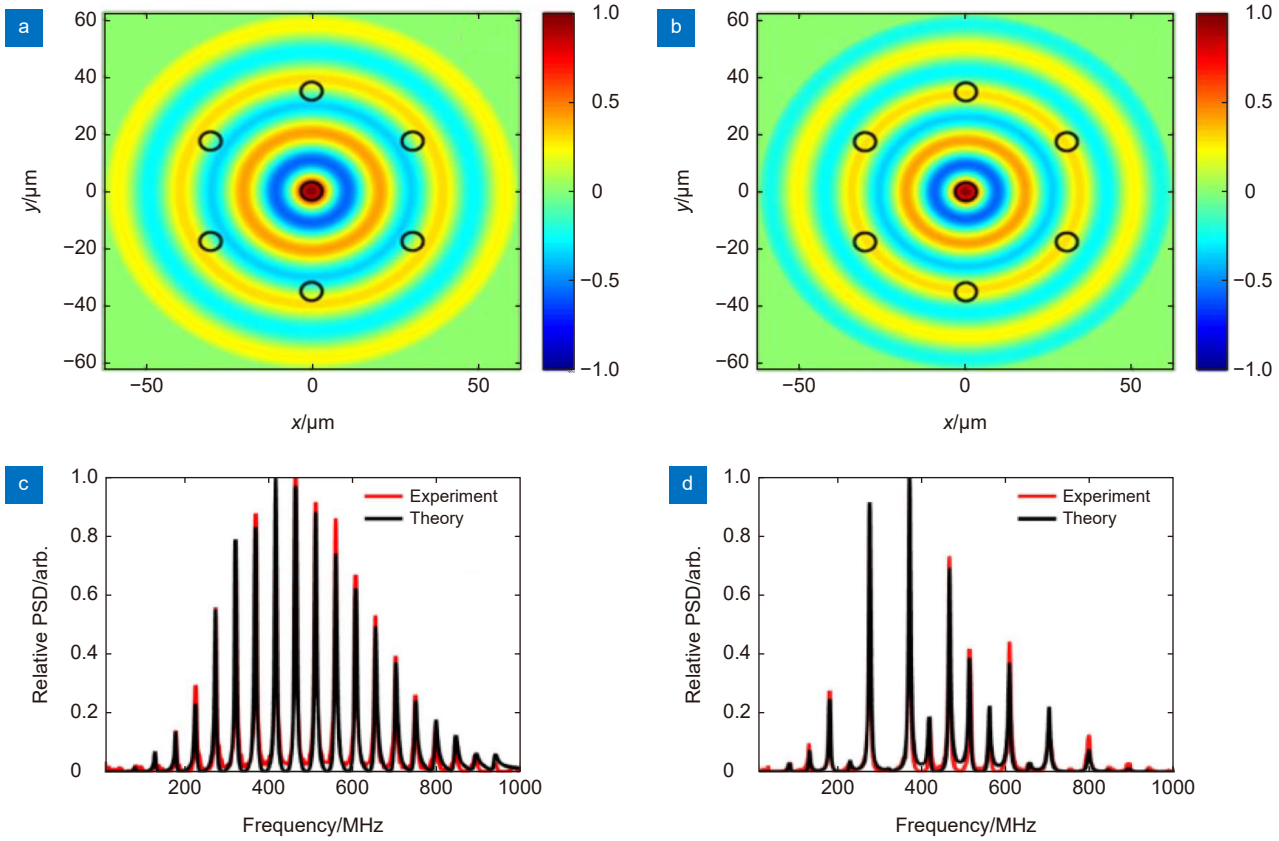

图 8 多芯光纤中的 F-SBS。(a), (b) $R_{0,7}$ 和 $R_{0,8}$ 模的位移场分布；
(c), (d) 主芯激发，分别在主芯和测芯测量的 F-SBS 谱[43]

Fig. 8 F-SBS in multi-core fiber. (a), (b) Transverse displacement profiles of modes $R_{0,7}$ and $R_{0,8}$;
(c), (d) F-SBS spectrums measured in the inner core and outer core. The excitation light propagates in the inner core[43]

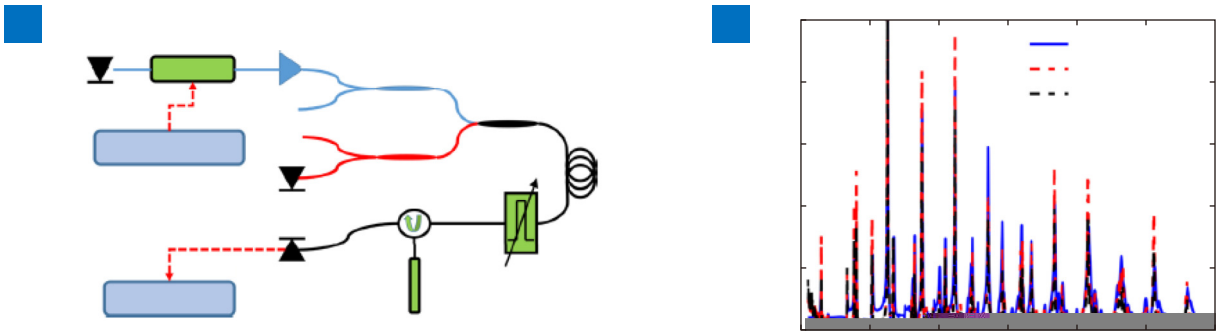

图 9 保偏光纤中的 F-SBS。(a) 实验装置图；(b) 实验结果。红色结果对应快轴激发慢轴探测，黑色结果相反[41]

Fig. 9 F-SBS in polarization maintaining fiber. (a) Experimental set-up; (b) Measured F-SBS spectrums. The red trace is measured when the excitation light propagating in the fast axis, and probe in the slow axis; The black trace is measured in the opposite situation[41]

2018 Thévenaz 500 ns

F-SBS

730 m 30 m 10 ns

F-SBS [36] 11

F-SBS

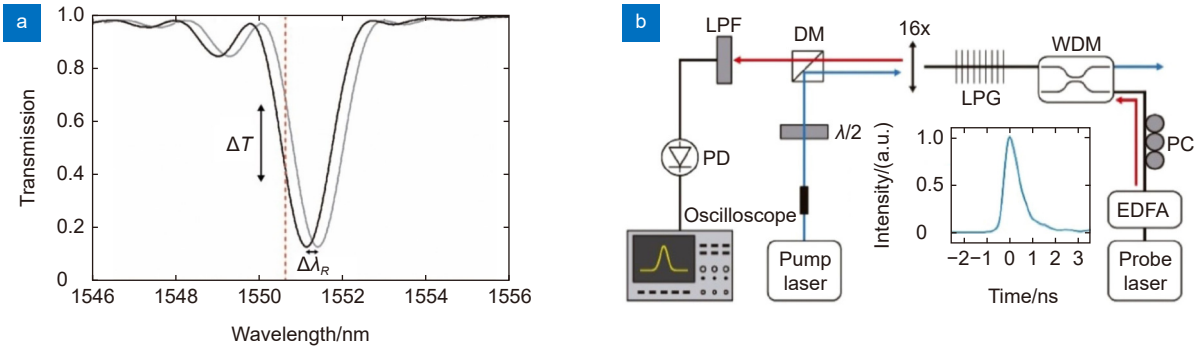

图 10 LPG 用于解调 F-SBS。(a) 原理示意图；(b) 实验装置图[45]

Fig. 10 F-SBS demodulation by LPG. (a) Schematic diagram; (b) Experimental set-up[45]

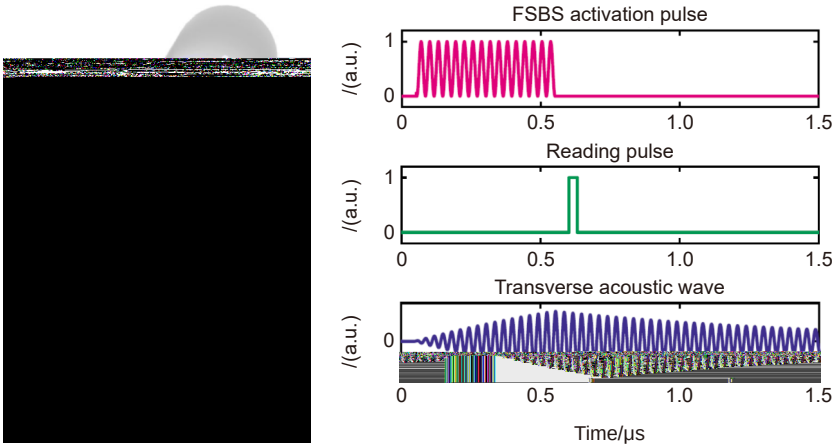

图 11 基于本地光相位追溯技术的分布式 F-SBS 测量。激发光与探测光不仅在波长上不同，也在时间上区分[36]

Fig. 11 Distributed F-SBS sensor based on local light phase recovery. The excitation and probe pulses are not only separated by wavelength, but also by time[36]

F-SBS

$$\begin{aligned} E(\Omega,z,t) &= A(z,t)\exp[\mathrm{j}(kz-\omega t+\varphi_0)] \\ &\quad \cdot \exp[\mathrm{j}\Delta\varphi(\Omega,z)\cos(\Omega t)] \\ &= A(z,t)\exp[\mathrm{j}(kz-\omega t+\varphi_0)] \\ &\quad \cdot \left[\sum_{n=-\infty}^{\infty} \mathrm{j}^n \mathrm{J}_n(\Delta\varphi(\Omega,z))\exp(\mathrm{j}n\Omega t)\right], \end{aligned} \tag{17}$$

$\Delta\varphi(\Omega,z)$ z Ω

$$\mathrm{J}_{n-1}(\Delta\varphi(\Omega,z)) + \mathrm{J}_{n+1}(\Delta\varphi(\Omega,z)) = \frac{2n\mathrm{J}_n(\Delta\varphi(\Omega,z))}{\Delta\varphi(\Omega,z)}. \tag{18}$$

$n = 1$

$$\begin{aligned} \Delta\varphi(\Omega,z) &= 2\left(\frac{\mathrm{J}_1(\Delta\varphi(\Omega,z))}{\mathrm{J}_0(\Delta\varphi(\Omega,z)) + \mathrm{J}_2(\Delta\varphi(\Omega,z))}\right) \\ &= 2\left(\frac{\sqrt{I^{(1)}(\Delta\varphi(\Omega,z))}}{\sqrt{I^{(0)}(\Delta\varphi(\Omega,z))} + \sqrt{I^{(2)}(\Delta\varphi(\Omega,z))}}\right), \end{aligned} \tag{19}$$

$I^{(i)}(\Delta\varphi(\Omega,z))$ i

+1 +2

F-SBS

SBS

Thévenaz

730 m

500 m 30 m

F-SBS

B-SBS

30 ns

3 m 12

15 m

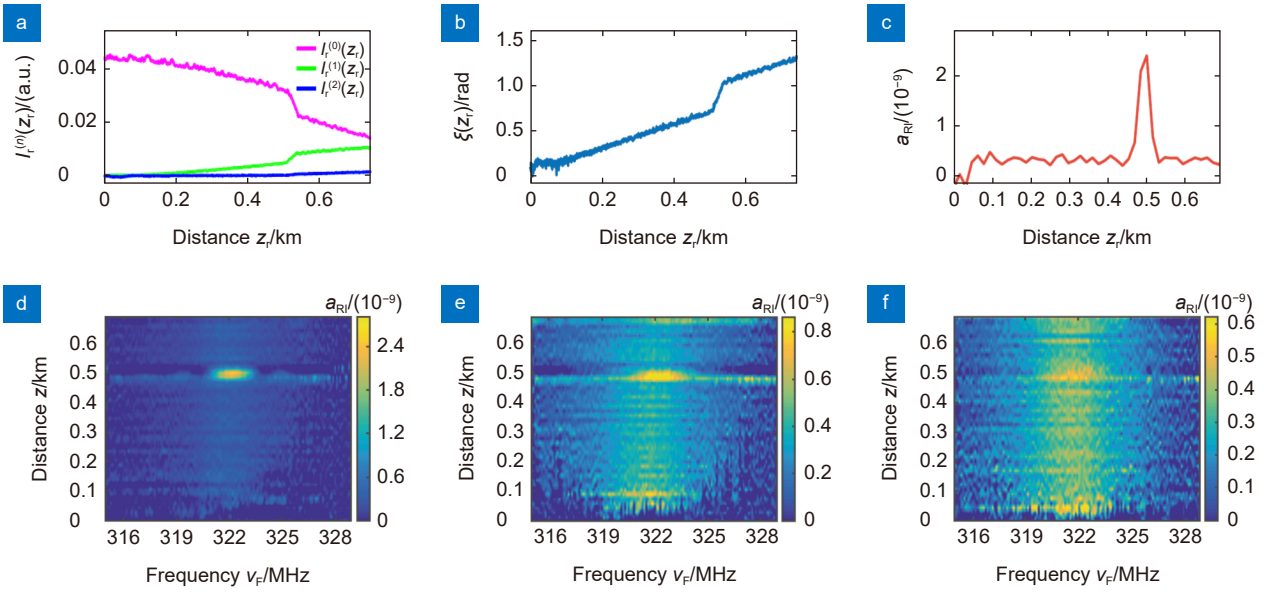

图 12 信号处理过程与实验结果。(a) 测量得到各阶边带光强的空间分布情况；(b) 还原出相位调制随距离的累积情况；(c) 微分得到的分布式相移结果；(d)~(e) 待测光纤置于空气、酒精和水中的测得的分布式 F-SBS 谱[36]

Fig. 12 Distributed F-SBS sensor based on local light phase recovery. (a) Distributed light intensity of 0, +1 and +2-order sidebands; (b) Phase accumulation along the fiber; (c) Distributed phase shift demodulated by differentiation; (d)~(f) Distributed F-SBS spectrums measured when the fiber under test placed in air, ethanol, and water[36]

2021 Thévenaz Serrodyne F-SBS [46]

0.8 m

3.2 基于能量转移的探测方案

2009 Kang F-SBS F-SBS [39] SBS

$U(z,t)$ E_i ρ $A_i(z,t)$

$$E_i(r,z,t)=E_0(r)A_i(z,t)\mathrm{e}^{\mathrm{j}(\omega_i t-k_i z)+c.c.}, \tag{20}$$

$$\rho(r,z,t)=\rho_0(r)U(z,t)\mathrm{e}^{\mathrm{j}(\Omega t-qz)+c.c.}, \tag{21}$$

$i=1,2$ $\omega_1-\omega_2=\Omega$

$$\frac{\partial^2 E}{\partial z^2}-\frac{n_{\mathrm{eff}}}{c}\frac{\partial^2 E}{\partial t^2}=\frac{1}{\varepsilon_0 c^2}\frac{\partial^2 P^{\mathrm{NL}}}{\partial t^2}, \tag{22}$$

$$\frac{\partial^2\rho}{\partial t^2}-\bar{\Gamma}\nabla^2\frac{\partial\rho}{\partial t}-v_{\mathrm{L}}{}^2\nabla^2\rho$$
$$=\nabla\cdot f=-\frac{1}{2}\varepsilon_0(a_1+4a_2)\nabla^2(E_1E_2{}^*). \tag{23}$$

(20) (21) (22) (23)

$$\frac{\partial A_1}{\partial z}=\frac{\mathrm{j}\omega_1 Q_{\mathrm{PE}}}{2nc\bar{\rho}}A_2U$$

$$\frac{\partial A_2}{\partial z}=\frac{\mathrm{j}\omega_2 Q_{\mathrm{PE}}}{2nc\bar{\rho}}A_1U^*, \tag{24}$$

$$U(z)=\frac{\varepsilon_0 Q_{\mathrm{ES}}}{\Omega_{0,m}\Gamma_{0,m}[\mathrm{j}-2(\Omega-\Omega_{0,m})/\Gamma_{0,m}]}A_1A_2{}^*. \tag{25}$$

$$\frac{\partial A_1}{\partial z}=-\frac{\mathrm{j}\omega_1\varepsilon_0 Q_{\mathrm{ES}}Q_{\mathrm{PE}}}{2\bar{\rho}nc\Omega_{0,m}\Gamma_{0,m}[\mathrm{j}-2(\Omega-\Omega_{0,m})/\Gamma_{0,m}]}A_1|A_2|^2,$$

$$\frac{\partial A_2}{\partial z}=\frac{\mathrm{j}\omega_2\varepsilon_0 Q_{\mathrm{ES}}Q_{\mathrm{PE}}}{2\bar{\rho}nc\Omega_{0,m}\Gamma_{0,m}[\mathrm{j}-2(\Omega-\Omega_{0,m})/\Gamma_{0,m}]}A_2|A_1|^2. \tag{26}$$

$P=2nc\varepsilon_0|A|^2$

$$\frac{\mathrm{d}P_1(\Omega,z)}{\mathrm{d}z}=-\frac{\omega_1 Q_{\mathrm{ES}} Q_{\mathrm{PE}}}{2\bar{\rho}n^2c^2\Omega_{0,m}\Gamma_{0,m}}\cdot\frac{(\Gamma_{0,m}/2)^2}{(\Gamma_{0,m}/2)^2+(\Omega-\Omega_{0,m})^2}P_1(z)P_2(z)=-g_{0,m}^{(\Omega)}P_1(z)P_2(z),$$

$$\frac{\mathrm{d}P_2(\Omega,z)}{\mathrm{d}z}=\frac{\omega_2 Q_{\mathrm{ES}} Q_{\mathrm{PE}}}{2\bar{\rho}n^2c^2\Omega_{0,m}\Gamma_{0,m}}\cdot\frac{(\Gamma_{0,m}/2)^2}{(\Gamma_{0,m}/2)^2+(\Omega-\Omega_{0,m})^2}P_1(z)P_2(z)=g_{0,m}^{(\Omega)}P_1(z)P_2(z), \tag{27}$$

$$g_{0,m}^{(\Omega)}(\Omega,z)=g_{0,m}\frac{(\Gamma_{0,m}/2)^2}{(\Gamma_{0,m}/2)^2+(\Omega-\Omega_{0,m})^2}. \tag{28}$$

$g_{0,m}^{(\Omega)}(\Omega,z)$ $P_1(\Omega,z)$ $P_2(\Omega,z)$

$$g_{0,m}^{(\Omega)}(\Omega,z)=\frac{P_1(\Omega,z)}{P_2(\Omega,z)[P_1(\Omega,z)+P_2(\Omega,z)]}\cdot\frac{\mathrm{d}[P_2(\Omega,z)/P_1(\Omega,z)]}{\mathrm{d}z}. \tag{29}$$

P_1 P_2

F-SBS

F-SBS

2018 Zadok

[47]

(optical time-domain reflectometry, OTDR)

(optomechanical time-domain reflectometry, OM-TDR)

13

F-SBS

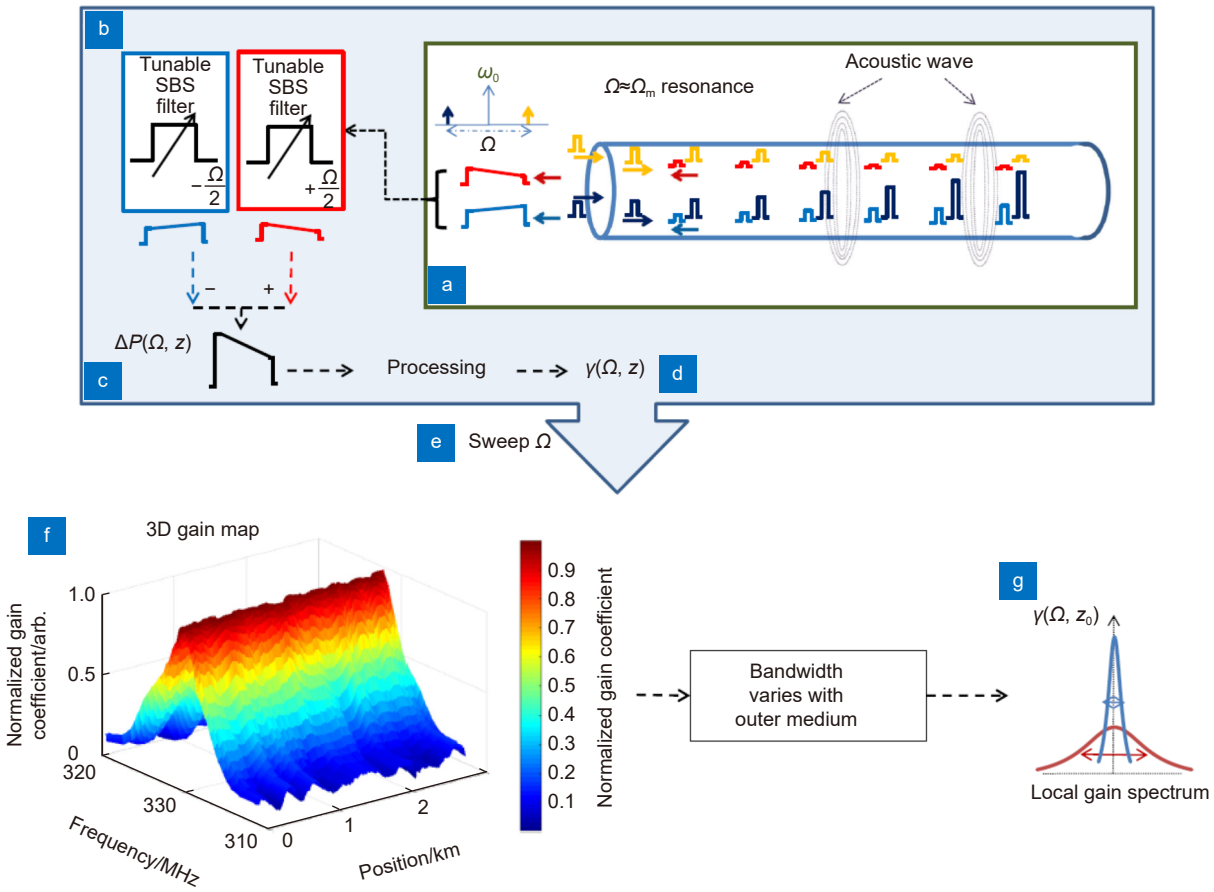

图 13 OMTDR 传感原理。用于探测的双频脉冲在传输过程中不断转移能量，其背向瑞利散射信号携带分布式光强信息[47]

Fig. 13 Principle of OMTDR. The energy transferred between the dual-frequency components of the pulses, and their Rayleigh scattering lights are used to demodulation[47]

F-SBS

P_1 P_2

1 μs 3 km

$\Omega_{0,m}$ 100 m

Zadok 14

$\Omega_{\mathrm{BSBS}} \pm \Omega_{0,m}/2$

$g_{0,m}^{(\Omega)}(\Omega, z)$ F-SBS

F-SBS

$P_{1,2}$

Zadok F-SBS

2020 F-SBS

$\mathrm{R}_{0,m}$ —— (opto-mechanical

1 μs time-domain analysis, OMTDA)[35]

100 m

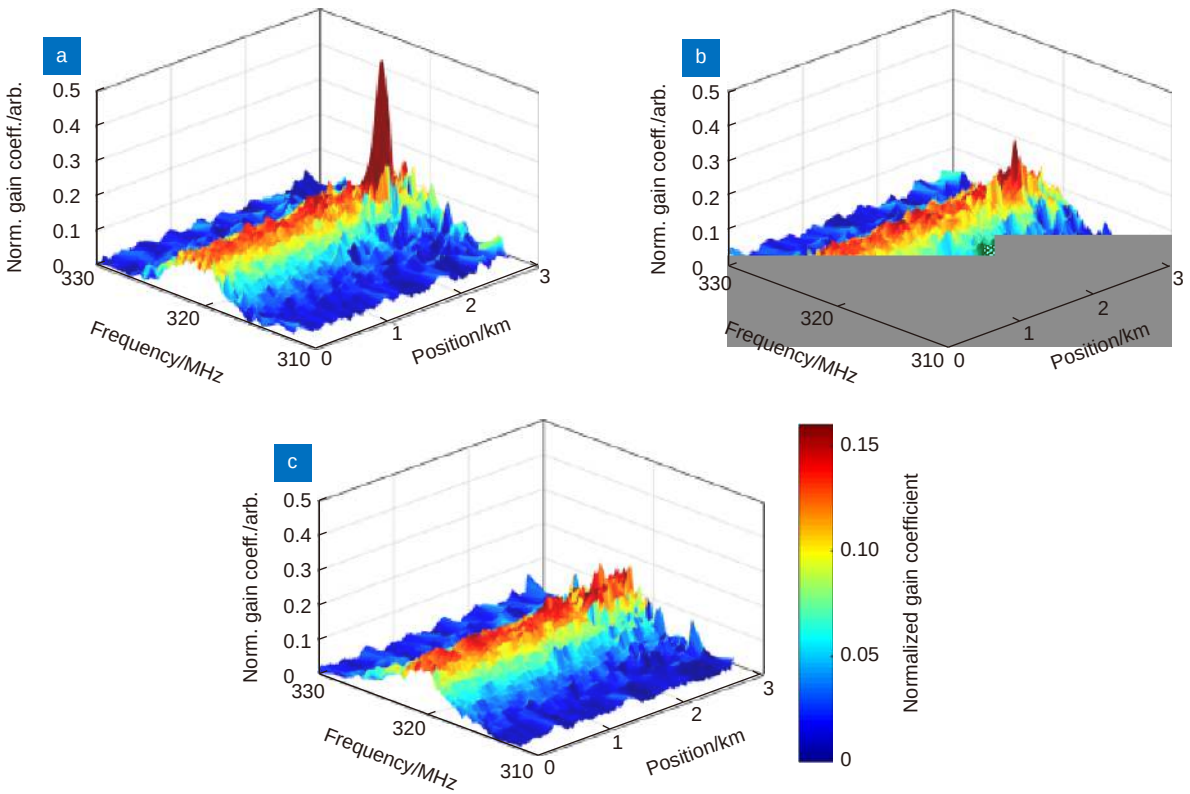

图 14 OMTDR 的分布式传感结果。(a)~(c) 分别为待测光纤段置于空气、酒精和水中的分布式 F-SBS 谱[47]

Fig. 14 Distributed sensing results of OMTDR. (a)~(c) are the distributed F-SBS spectrums measured when the fiber under test placed in air, ethanol, and water[47]

F-SBS

10 ns(

TAW 1 m)

225 m

TAW 25 m

5 m 16

15 17 18

F-SBS 0.45 MHz

2.21 MHz

TAW 1 m

OMTDA 2 m

(5) F-SBS

OMTDA

TAW [12] 19

BOTDA

3.9 nm

BOTDA (~100 nm)

F-SBS 2021

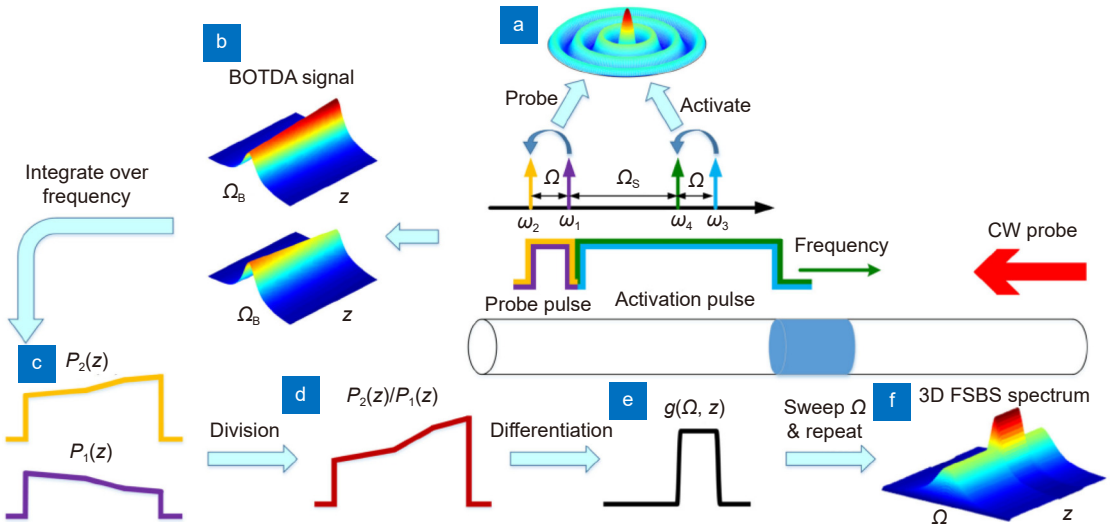

图 15 OMTDA 技术原理图[35]

Fig. 15 Schematic diagram of OMTDA[35]

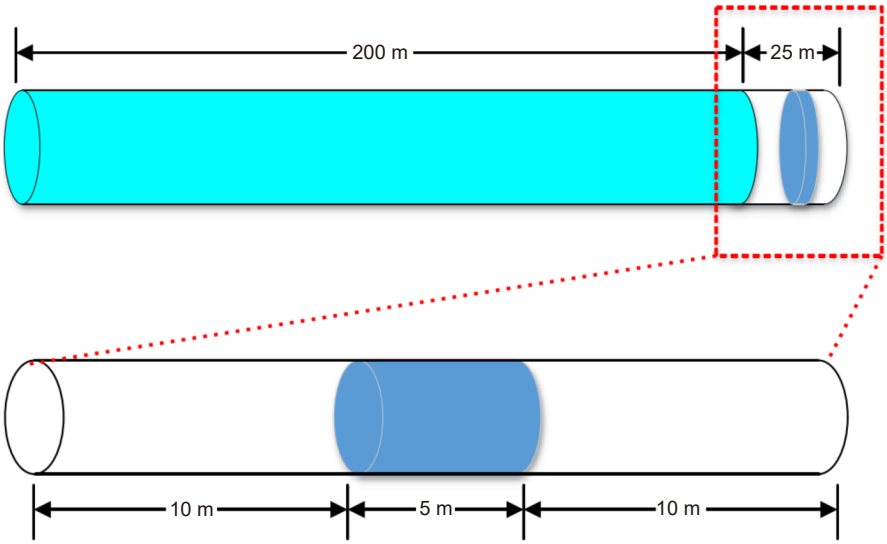

图 16 传感光纤示意图[48]

Fig. 16 Schematic diagram of the fiber under test[48]

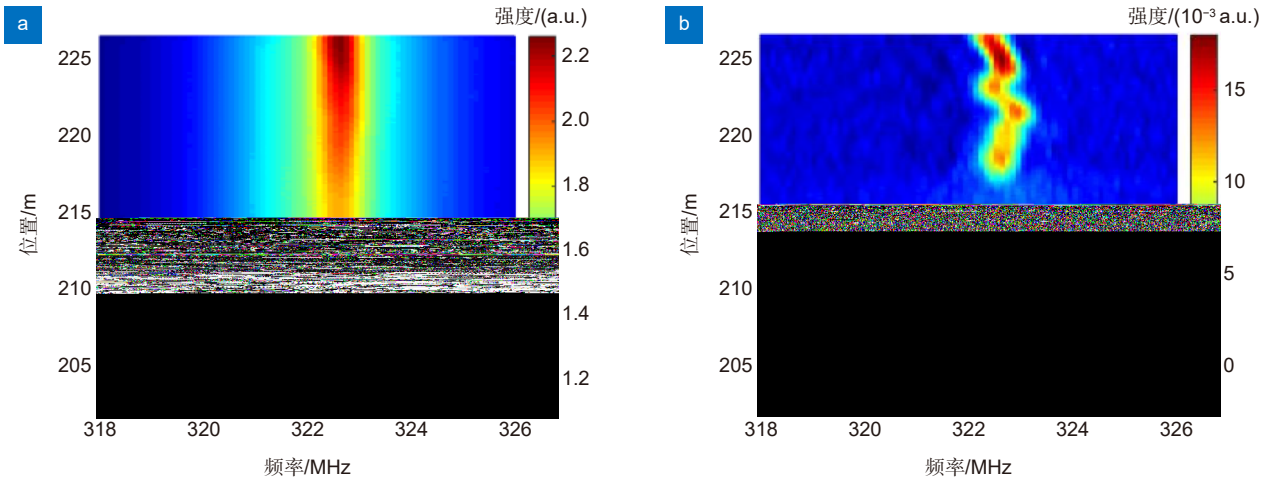

图 17 分布式测量结果。(a) 能量转移的累积过程；(b) 分布式 F-SBS 增益谱[48]

Fig. 17 Distributed results of OMTDA. (a) The energy transfer process along the fiber; (b) Distributed F-SBS gain spectrum[48]

OMTDA 0.8 m

[49] 20

B-SBS

OMTDA 0.8 m

F-SBS

OMTDA

F-SBS

(polarization beam splitter,

PBS)

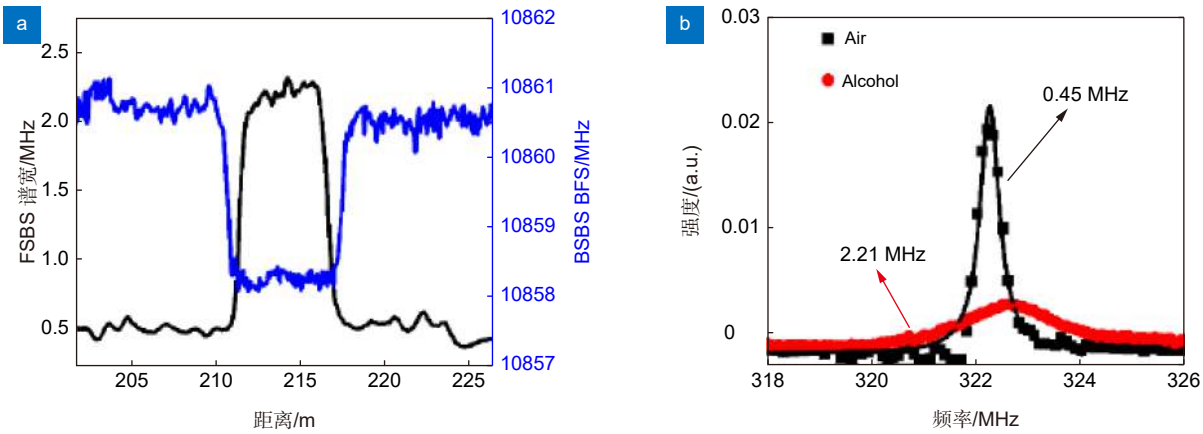

图 18 声阻抗传感结果。

(a) F-SBS 谱宽分布;

(b) 空气和酒精中的 F-SBS 增益谱[48]

Fig. 18 Results of acoustic impedance sensing.

(a) The linewidth of spectrums along the fiber;

(b) F-SBS spectrums measured in air and ethanol[48]

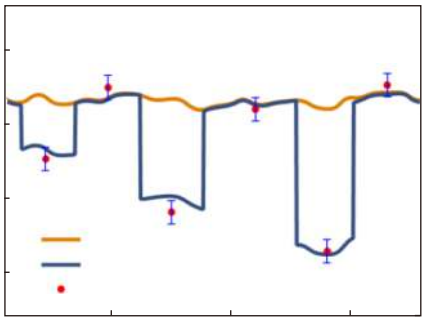

图 19 分布式光纤直径测量结果[12]。

(a) 腐蚀前后解调出的光纤直径及电镜对比;

(b) 待测光纤的直径分布; (c) A、B、C、E 处截面的电镜图像

Fig. 19 Results of distributed diameter measurements[12].

(a) Diameter distribution before and after etching and its comparison with the SEM results (A-F);

(b) Diameter variations along the FUT;

(c) Representative images of the fiber cross section at A, B, C and E captured by SEM

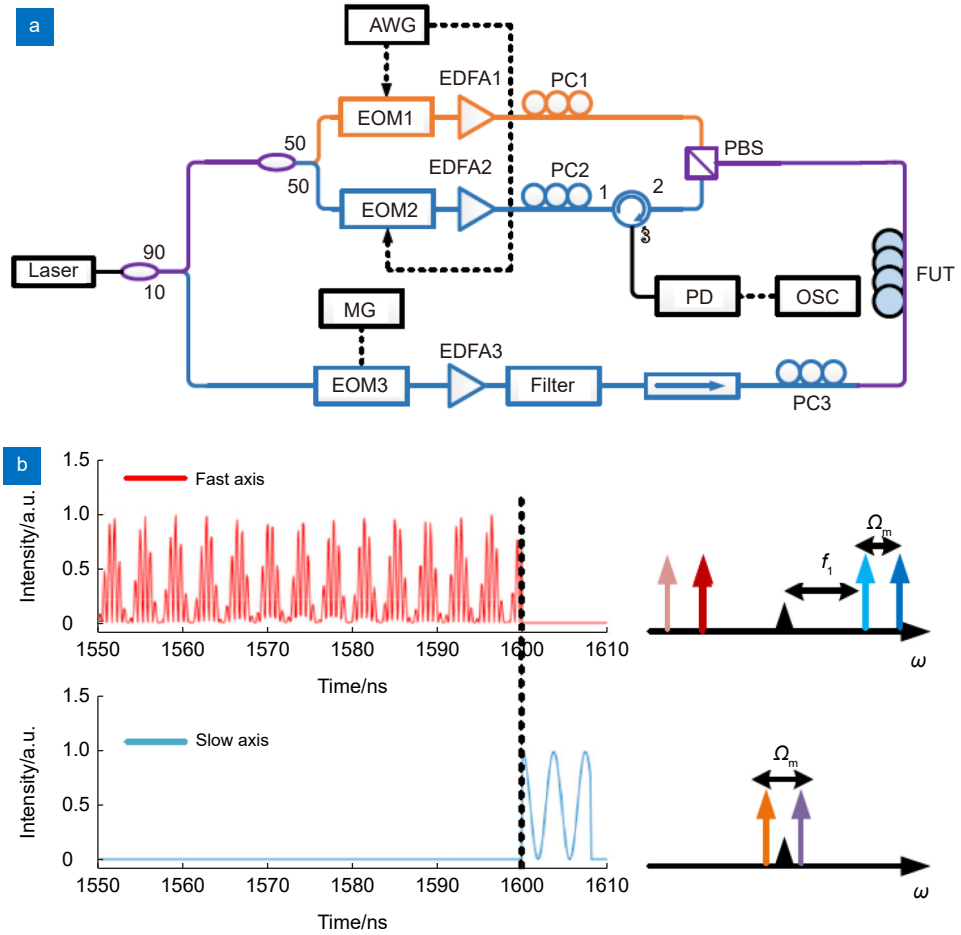

图 20 (a) 偏振分极 OMTDA 装置图；(b) 激发脉冲和读取脉冲的时频域示意图[49]

Fig. 20 (a) Experimental setup for polarization separation assisted OMTDA; (b) Temporal trace and frequency components of activation and probing pulses[49]

4 结论和展望

F-SBS

F-SBS

—— F-SBS

F-SBS F-SBS

参考文献

[1] Dong Y K. High-performance distributed brillouin optical fiber sensing[J]. *Photonic Sens*, 2021, **11**(1): 69−90.

[2] Liu T, Li H, He T, et al. Ultra-high resolution strain sensor network assisted with an LS-SVM based hysteresis model[J]. *Opto-Electron Adv*, 2021, **4**(5): 200037.

[3] Guan B O, Jin L, Ma J, et al. Flexible fiber-laser ultrasound sensor for multiscale photoacoustic imaging[J]. *Opto-Electron Adv*, 2021, **4**(8): 200081.

[4] Zhang L, Pan J, Zhang Z, et al. Ultrasensitive skin-like wearable optical sensors based on glass micro/nanofibers[J]. *Opto-Electron Adv*, 2020, **3**(3): 190022.

[5] Tan F Z, Lyu W, Chen S Y, et al. Contactless vital signs monitoring based on few-mode and multi-core fibers[J]. *Opto-Electron Adv*, 2020, **3**(5): 190034.

[6] Liu S Q, Yu F H, Hong R, et al. Advances in phase-sensitive optical time-domain reflectometry[J]. *Opto-Electron Adv*, 2022, **5**(3): 200078.

[7] Zhang X Z, Yang B Y, Jiang J F, et al. Side-polished SMS based RI sensor employing macro-bending perfluorinated POF[J]. *Opto-Electron Adv*, 2021, **4**(10): 200041.

[8] Lou X T, Wang Y, Dong Y K. Multipoint dispersion

spectroscopic gas sensing by optical FMCW interferometry[J]. *Opt Lett*, 2021, **46**(23): 5950−5953.

[9] Lou X T, Feng Y B, Yang S H, et al. Ultra-wide-dynamic-range gas sensing by optical pathlength multiplexed absorption spectroscopy[J]. *Photonics Res*, 2021, **9**(2): 193−201.

[10] Shelby R M, Levenson M D, Bayer P W. Guided acoustic-wave brillouin scattering[J]. *Phys Rev B*, 1985, **31**(8): 5244−5252.

[11] Antman Y, Clain A, London Y, et al. Optomechanical sensing of liquids outside standard fibers using forward stimulated Brillouin scattering[J]. *Optica*, 2016, **3**(5): 510−516.

[12] Hua Z J, Ba D X, Zhou D W, et al. Non-destructive and distributed measurement of optical fiber diameter with nanometer resolution based on coherent forward stimulated Brillouin scattering[J]. *Light Adv Manuf*, 2021, **2**(4): 373−384.

[13] Sánchez L A, Díez A, Cruz J L, et al. High accuracy measurement of Poisson's ratio of optical fibers and its temperature dependence using forward-stimulated Brillouin scattering[J]. *Opt Express*, 2022, **30**(1): 42−52.

[14] Tanaka Y, Ogusu K. Temperature coefficient of sideband frequencies produced by depolarized guided acoustic-wave Brillouin scattering[J]. *IEEE Photonics Technol Lett*, 1998, **10**(12): 1769−1771.

[15] Tanaka Y, Ogusu K. Tensile-strain coefficient of resonance frequency of depolarized guided acoustic-wave Brillouin scattering[J]. *IEEE Photonics Technol Lett*, 1999, **11**(7): 865−867.

[16] Brillouin L. Diffusion de la lumière et des rayons X par un corps transparent homogène: Influence de l'agitation thermique[J]. *Ann Phys*, 1922, **9**(17): 88−122.

[17] Gross E. The splitting of spectral lines at scattering of light by liquids[J]. *Nature*, 1930, **126**(3176): 400.

[18] Yuan D P, Chen P, Mao Z H, et al. Ocean mixed layer depth estimation using airborne Brillouin scattering lidar: simulation and model[J]. *Appl Opt*, 2021, **60**(36): 11180−11188.

[19] Wei W, Mao Z, Sun N Y, et al. High pressure-temperature single-crystal elasticity of grossular: implications for the low-velocity layer in the bottom transition zone[J]. *Geophys Res Lett*, 2021, **48**(9): e2021GL093540.

[20] Horiguchi T, Tateda M. BOTDA - nondestructive measurement of single-mode optical fiber attenuation characteristics using brillouin interaction: theory[J]. *J Light Technol*, 1989, **7**(8): 1170−1176.

[21] Parker T R, Farhadiroushan M, Handerek V A, et al. Temperature and strain dependence of the power level and frequency of spontaneous Brillouin scattering in optical fibers[J]. *Opt Lett*, 1997, **22**(11): 787−789.

[22] Dong Y K, Zhang H Y, Chen L, et al. 2 cm spatial-resolution and 2 km range Brillouin optical fiber sensor using a transient differential pulse pair[J]. *Appl Opt*, 2012, **51**(9): 1229−1235.

[23] Dong Y K, Ba D X, Jiang T F, et al. High-spatial-resolution fast BOTDA for dynamic strain measurement based on differential double-pulse and second-order sideband of modulation[J]. *IEEE Photonics J*, 2013, **5**(3): 2600407.

[24] Ba D X, Li Y, Yan J L, et al. Phase-coded Brillouin optical correlation domain analysis with 2-mm resolution based on phase-shift keying[J]. *Opt Express*, 2019, **27**(25): 36197−36205.

[25] Wang B Z, Ba D X, Chu Q, et al. High-sensitivity distributed dynamic strain sensing by combining Rayleigh and Brillouin scattering[J]. *Opto-Electron Adv*, 2020, **3**(12): 200013.

[26] Sittig E K, Coquin G A. Visualization of plane-strain vibration modes of a long cylinder capable of producing sound radiation[J]. *J Acoust Soc Am*, 1970, **48**(5B): 1150−1159.

[27] Thurston R N. Elastic waves in rods and clad rods[J]. *J Acoust Soc Am*, 1978, **64**(1): 1−37.

[28] Diamandi H H, Bashan G, London Y, et al. Interpolarization forward stimulated brillouin scattering in standard single-mode fibers[J]. *Laser Photonics Rev*, 2022, **16**(1): 2100337.

[29] Horiguchi T, Kurashima T, Tateda M. A technique to measure distributed strain in optical fibers[J]. *IEEE Photonics Technol Lett*, 1990, **2**(5): 352−354.

[30] Kurashima T, Horiguchi T, Tateda M. Thermal effects of brillouin gain spectra in single-mode fibers[J]. *IEEE Photonics Technol Lett*, 1990, **2**(10): 718−720.

[31] Wang J, Zhu Y H, Zhang R, et al. FSBS resonances observed in a standard highly nonlinear fiber[J]. *Opt Express*, 2011, **19**(6): 5339−5349.

[32] Chow D M, Thévenaz L. Forward Brillouin scattering acoustic impedance sensor using thin polyimide-coated fiber[J]. *Opt Letters*, 2018, **43**(21): 5467−5470.

[33] Diamandi H H, London Y, Bashan G, et al. Forward stimulated Brillouin scattering analysis of optical fibers coatings[J]. *J Lightw Technol*, 2021, **39**(6): 1800−1807.

[34] Diamandi H H, London Y, Bashan G, et al. Distributed opto-mechanical analysis of liquids outside standard fibers coated with polyimide[J]. *APL Photonics*, 2019, **4**(1): 016105.

[35] Pang C, Hua Z J, Zhou D W, et al. Opto-mechanical time-domain analysis based on coherent forward stimulated Brillouin scattering probing[J]. *Optica*, 2020, **7**(2): 176−184.

[36] Chow D M, Yang Z S, Soto M A, et al. Distributed forward Brillouin sensor based on local light phase recovery[J]. *Nat Commun*, 2018, **9**(1): 2990.

[37] Xu W Y, Zhou J, Hu J K. Ultrasonic attenuation and velocity on polymers[J]. *Chin J Mater Res*, 1989, **3**(3): 280−284.

, , .
[J]. , 1989, **3**(3): 280−284.

[38] Townsend P D, Poustie A J, Hardman P J, et al. Measurement of the refractive-index modulation generated by electrostriction-induced acoustic waves in optical fibers[J]. *Opt Lett*, 1996, **21**(5): 333−335.

[39] Kang M S, Nazarkin A, Brenn A, et al. Tightly trapped acoustic phonons in photonic crystal fibres as highly nonlinear artificial Raman oscillators[J]. *Nat Phys*, 2009, **5**(4): 276−280.

[40] Zheng Z, Li Z Y, Fu X L, et al. Multipoint acoustic impedance sensing based on frequency-division multiplexed forward stimulated Brillouin scattering[J]. *Opt Lett*, 2020, **45**(16): 4523−4526.

[41] Bashan G, Diamandi H H, London Y, et al. Forward stimulated Brillouin scattering and opto-mechanical non-reciprocity in standard polarization maintaining fibres[J]. *Light Sci Appl*, 2021, **10**(1): 119.

[42] Zhao Z Y, Tang M, Lu C. Distributed multicore fiber sensors[J]. *Opto-Electron Adv*, 2020, **3**(2): 190024.

[43] Diamandi H H, London Y, Zadok A. Opto-mechanical inter-core cross-talk in multi-core fibers[J]. *Optica*, 2017, **4**(3): 289−297.

[44] Diamandi H H, London Y, Bergman A, et al. Opto-mechanical interactions in multi-core optical fibers and their applications[J]. *IEEE J Sel Top Quantum Electron*, 2020, **26**(4): 2600113.

[45] Sánchez L A, Díez A, Cruz J L, et al. Efficient interrogation method of forward Brillouin scattering in optical fibers using a narrow bandwidth long-period grating[J]. *Opt Lett*, 2020, **45**(19): 5331−5334.

[46] Zaslawski S, Yang Z S, Thévenaz L. Distributed optomechanical fiber sensing based on serrodyne analysis[J]. *Optica*, 2021, **8**(3): 388−395.

[47] Bashan G, Diamandi H H, London Y, et al. Optomechanical time-domain reflectometry[J]. *Nat Commun*, 2018, **9**(1): 2991.

[48] Pang C. High spatial resolution sensing based on forward stimulated brillouin scattering[D]. Harbin: Harbin Institute of Technology, 2019.
. [D].
: , 2019.

[49] Ba D X, Hua Z J, Li Y J, et al. Polarization separation assisted optomechanical time-domain analysis with submeter resolution[J]. *Opt Lett*, 2021, **46**(23): 5886−5889.

作者简介

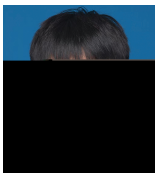

(1998-)

E-mail: litianfu3307@163.com

(1981-)

E-mail: aldendong@163.com

Recent progress in optical fiber sensing based on forward stimulated Brillouin scattering

Li Tianfu[1], Ba Dexin[1], Zhou Dengwang[1,2], Ren Yuli[1],
Chen Chao[1], Zhang Hongying[3], Dong Yongkang[1*]

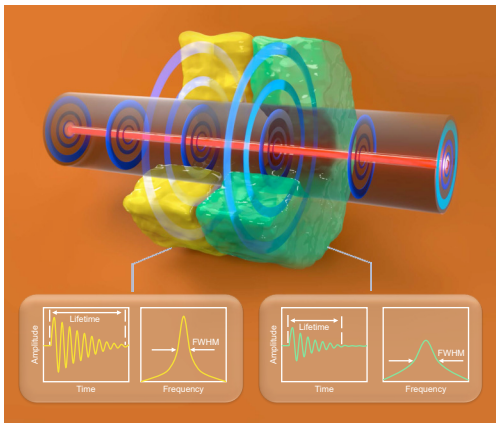

The schematic diagram of acoustic impedance sensing

Overview: The Brillouin optical fiber sensors have been well developed in the past decades, due to their capabilities of distributed sensing. With the introduction of new sensing mechanisms, the physical quantity can be measured by distributed Brillouin optical fiber sensors gradually increase. Forward stimulated Brillouin scattering (F-SBS) is one of the most typical representations of these new mechanisms, which allows unmarked substance identification with non-structures additional. The sensors based on F-SBS are expected to be used in pollution monitoring, chemical reaction monitoring, biomedical probes, and optical fiber manufacturing. The F-SBS sensors are promising methods for these and other applications which need high accuracy, and unmarked substance identification, and the distributed F-SBS sensors with the high spatial resolution are considered to greatly potential in the future.

In the micron-sized symmetrical shapes, just like optical fiber, acoustic waves can be transmitted in cross-sections, reflected on the boundary, and with resonant frequencies ranging from megahertz (MHz) to gigahertz (GHz). It is called the transverse acoustic wave (TAW). TAW hardly transmits in the axial direction. When stimulated by intense optical waves propagating in the fiber core through electro-strictive, TAW can be considered moving with the same speed as an optical wave at the axial direction, so that a phase modulation (PM) caused by TAW can be loaded on co-propagating light, and F-SBS occurred. The lifetime of TAW will be extended to several microseconds when the optical fiber is placed in the air, without coating, and hundreds of nanoseconds in the liquids, which have a strict relationship with the acoustic impedance of the outside substance. By demodulated F-SBS induced PM, TAW can be recovered, which can be used to get the acoustic impedance of the outside substance. What's more, the resonance frequency of the TAW is related to the diameter of the fiber, which allows an optical fiber diameter measurement method with high accuracy.

Distributed F-SBS sensors are considered as powerful tools on substance identification and optical fiber quality inspection, which means high accuracy and spatial resolution are necessary. In 2018, the distributed F-SBS sensor based on local light phase recovery is proposed, and measured F-SBS via phase demodulation, with a 30 m spatial resolution on a 730 m optical fiber. In the same year, opto-mechanical time-domain reflectometry based on measurement of energy transferring is proposed, which has 100 m spatial resolution on 3 km fiber. In 2020, the team proposed opto-mechanical time-domain analysis (OMTDA), a 2 m spatial resolution on a 225 m fiber was achieved, and in 2021, polarization separate assisted OMTDA was proposed, with a spatial resolution of 0.8 m. The performance of distributed F-SBS sensors is ameliorated rapidly these few years.

In summary, the basic principle, sensing scheme, and performance of F-SBS optical fiber sensors are introduced in this paper. With the F-SBS sensor applied in practice, increasing demand for high accuracy, and high spatial resolution emerges, which we believe will be dominant in the research of substance identification sensors in the future.

Li T F, Ba D X, Zhou D W, et al. Recent progress in optical fiber sensing based on forward stimulated Brillouin scattering[J]. *Opto-Electron Eng*, 2022, **49**(9): 220021; DOI: 10.12086/oee.2022.220021

Foundation item: National Natural Science Foundation of China (62075051, 61975045) and Natural Science Foundation of Heilongjiang Province (LH2020F014)

[1]National Key Laboratory of Science and Technology on Tunable Laser, Harbin Institute of Technology, Harbin, Heilongjiang 150001, China; [2]Postdoctoral Research Station for Optical Engineering & Research Center for Space Optical Engineering, Harbin Institute of Technology, Harbin, Heilongjiang 150001, China; [3]Heilongjiang Provincial Key Laboratory of Quantum Control, School of Measurement and Communication Engineering, Harbin University of Science and Technology, Harbin, Heilongjiang 150080, China

* E-mail: aldendong@163.com